Estimates of absolute crown strength and bite force in the lower postcanine dentition of Gigantopithecus blacki

Zhixing Yi, Clément Zanolli, Wei Liao, Wei Wang

Estimates of absolute crown strength and bite force in the lower postcanine dentition of *Gigantopithecus blacki*

Zhixing Yi [a b], Clément Zanolli [c], Wei Liao [a], Wei Wang [a]

[a] Institute of Cultural Heritage, Shandong University, Qingdao, 266237, China
[b] Guangxi Academy of Sciences, Beihai, 536000, China
[c] Univ. Bordeaux, CNRS, MCC, PACEA, UMR 5199, F-33600 Pessac, France

Corresponding author.
wangw@sdu.edu.cn

Abstract
Gigantopithecus blacki is hypothesized to have been capable of processing mechanically challenging foods, which likely required this species to have high dental resistance to fracture and/or large bite force. To test this hypothesis, we used two recently developed approaches to estimate absolute crown strength and bite force of the lower postcanine dentition. Sixteen *Gigantopithecus* mandibular permanent cheek teeth were scanned by micro-computed tomography. From virtual mesial cross-sections, we measured average enamel thickness and bi-cervical diameter to estimate absolute crown strength, and cuspal enamel thickness and dentine horn angle to estimate bite force. We compared *G. blacki* with a sample of extant great apes (*Pan*, *Pongo*, and *Gorilla*) and australopiths (*Australopithecus anamensis*, *Australopithecus afarensis*, *Australopithecus africanus*, *Paranthropus robustus*, and *Paranthropus boisei*). We also evaluated statistical differences in absolute crown strength and bite force between the premolars and molars for *G. blacki*. Results reveal that molar crown strength is absolutely greater, and molar bite force absolutely higher, in *G. blacki* than all other taxa except *P. boisei*, suggesting that *G. blacki* molars have exceptionally high resistance to fracture and the ability to generate exceptionally high bite force. In addition, *G. blacki* premolars have comparable absolute crown strength and larger bite force capabilities compared with its molars, implying possible functional specializations in premolars. The dental specialization of *G. blacki* could thus represent an adaptation to further facilitate the processing of mechanically challenging foods. While it is currently not possible to determine which types of foods were actually consumed by *G. blacki* through this study, direct evidence (e.g. dental chipping and microwear) left by the foods eaten by *G. blacki* could potentially lead to greater insights into its dietary ecology.
Keywords: Chuifeng Cave; Mohui Cave; Dietary adaption; Mechanically challenging foods; Fallback foods

1. Introduction
In 1935, von Koenigswald described a huge, high-crowned molar that he purchased from a Chinese drugstore in Hong Kong and found this molar to present distinctive features compared to other known primate teeth and erected the species *Gigantopithecus blacki* for it (Von Koenigswald, 1935). Evidence accumulated since then reveals that this extinct giant ape is the largest primate ever discovered (Zhang and Harrison, 2017). Most of the *G. blacki* specimens come from South China (Pei and Woo, 1956; Woo, 1962; Zhang, 1982; Wang, 2009; Jin et al., 2009, 2014; Zhao and Zhang, 2013; Wang et al., 2017; Zhang and Harrison, 2017), while a few isolated teeth from North Vietnam (Ciochon et al., 1996), North Thailand (Bocherens et al., 2017), and Java (Noerwidi et al., 2016; Zanolli et al., 2019) have also been reported. Over the

past six decades, nearly two thousand isolated teeth as well as four partial mandibles have been unearthed from ongoing cave excavations across South China (Zhang and Harrison, 2017). The estimated age of *G. blacki* ranges from ~2.0 Ma to ~300 ka (initial Early Pleistocene to Middle Pleistocene), as indicated by associated faunal assemblages and direct dating methods (Sun et al., 2014; Shao et al., 2014, 2015, 2017). Since the initial discovery of *G. blacki*, its phylogenetic relationship has been questioned. *Gigantopithecus blacki* was once considered to be a hominin (Weidenreich, 1945; Broom and Schepers, 1946; Gelvin, 1980; Zhang and Zhao, 2013). However, some also considered it to be a specialized great ape, with a possible close affinity to the *Sivapithecus–Indopithecus* clade (Pei and Woo, 1956; Pilbeam, 1970; Miller et al., 2008; Olejniczak et al., 2008a; Begun, 2010). Recently, Welker et al. (2019) successfully extracted dental proteins from *G. blacki* molar enamel and demonstrated that this species was an early diverging pongine.

Attempts have been made to determine the dietary behavior of *G. blacki* through a variety of approaches, such as dentognathic morphology (e.g. enamel thickness, tooth root length, occlusal area, and mandibular corpus depth; Woo, 1962; Olejniczak et al., 2008a; Kupczik and Dean, 2008; Zhang and Zhao, 2013; Kono et al., 2014; Zhang and Harrison, 2017), stable isotope analysis (Nelson, 2014; Qu et al., 2014; Bocherens et al., 2017; Jiang et al., 2021; Hu et al., 2022), dental microwear (Daegling and Grine, 1994; Zhao and Zhang, 2013), incidence of dental caries (Han and Zhao, 2002; Wang, 2009), analysis of phytoliths (Ciochon et al., 1990), and analysis of starch grains (Qu, 2014). These studies provided indications—e.g. enhanced enamel stability reflected by high calcium (Ca) isotope values, possibly being adapted to the consumption of hard foods (Hu et al., 2022)—that *G. blacki* may have been capable of processing mechanically challenging foods (MCFs), i.e. tough foods (Dickson, 2003; Olejniczak et al., 2008a; Kono et al., 2014) and/or hard foods (Kupczik and Dean, 2008; Qu, 2014; Hu et al., 2022). Feeding on tough or hard foods may require high dental resistance to fracture associated with repetitive and/or intense loading, respectively, while feeding on hard foods may further require relatively large bite force (BF). However, relatively few quantitative studies have investigated these dental biomechanical properties for *G. blacki* (e.g. Kupczik and Dean, 2008). Here, we address the following questions: 1) can the teeth of *G. blacki* resist breakage when processing MCFs and 2) does *G. blacki* have absolutely larger BF than extant apes and australopiths?

Schwartz et al. (2020) and Chai (2018) recently derived methods to estimate tooth resistance to fracture and BF, respectively. Schwartz et al. (2020) proposed a new metric, absolute crown strength (ACS), as a proxy for assessing tooth resistance to fracture. This parameter can be readily measured on the mesial section of a tooth. Estimating ACS involves two dental anatomical variables, i.e. average enamel thickness (AET) and bi-cervical diameter. In the Schwartz et al. (2020) study, tooth crown strength was reflected by two indices. One is the critical force (denoted by P_{RF}) needed to fully propagate a radial-median fracture from cusp to cervix, and the other is the critical force (denoted by P_{MF}) needed to fully propagate a margin fracture from cervix to cusp. Dental radial-median fractures can only be caused by biting on hard food items, while margin fractures can be induced by biting on hard or soft objects (Schwartz et al., 2020). The higher the tooth crown strength, the larger the critical force needed to cause radial-median fractures or margin fractures, and thus the larger the P_{RF} and P_{MF}. Both P_{RF} (Supplementary Online Material [SOM] S1) and P_{MF} (SOM S1) can be estimated according to the formulae derived by Lawn and Lee (2009). It is worth mentioning that in the biomechanical work of Lawn and Lee (2009), a tooth was modeled as a simplified dome-like structure with an equal-thickness enamel layer sitting atop a semicircular dentine base. To test whether ACS is a

significant predictor of tooth crown strength (i.e. P_{RF} and P_{MF}), Schwartz et al. (2020) estimated ACS, P_{RF}, and P_{MF} for a sample of 139 extant hominoid and extinct hominin mandibular molars and then performed least squares regressions between ACS and P_{RF}, and between ACS and P_{MF}. Results showed that ACS exhibited significant linear correlations with both P_{RF} and P_{MF} (with $r^2 > 0.86$), indicating that ACS is strongly correlated with the Lawn and Lee (2009) force estimates of tooth fracture.

In the numerical model proposed by Chai (2018), a tooth cusp was modeled as a truncated cone characterized by equal-thickness enamel layer that rests on conical-like dentine base (Chai, 2018: Fig. 4), which is different from the scheme for deriving ACS (Lawn and Lee, 2009; Schwartz et al., 2020). In addition, occlusal loading was simulated as a tooth cusp biting on a hard particle entrapped at the central fossa of the opposing tooth. With these simplifications on cusp structure and occlusal loading form, Chai (2018) conducted a series of finite element analyses (FEAs) to evaluate the conditions for cusp failure under occlusal loading. Simulation results showed that 1) tensile stresses were greater at the enamel–dentine junction (EDJ) and the peak stress occurred slightly below the dentine horn tip and 2) BF was correlated with two dental anatomical parameters: cusp enamel thickness and dentine horn angle (DHA). In parallel with the numerical simulations, Chai (2018) carried out tooth fracture tests to examine the reliability of the numerical model. Specifically, the polished cusps of human maxillary molars were subjected to axial occlusal force loaded by a tungsten carbide ball. After unloading, teeth were cut open to observe internal crack patterns. Internal cracking patterns showed general consistency with the numerical simulation results. For instance, in both cases, the enamel cracks extended from the EDJ and the peak stress occurred near the EDJ. Thus, despite underlying assumptions and limitations, the simplifications in the numerical model were deemed acceptable (Chai, 2018, 2020). Although there are other methods to estimate BF, most require cranial material (e.g. Demes and Creel, 1988; O'Connor et al., 2005; Wroe et al., 2010; Constantino et al., 2010; Eng et al., 2013) and are not suitable for the current study because no cranial remains of *G. blacki* have been found.

To test the hypothesis that *G. blacki* was capable of processing MCFs, we adopted the methods of Schwartz et al. (2020) and Chai (2018) to estimate ACS and BF, respectively. We then compared ACS and BF between *G. blacki* and a sample of extant great apes and extinct australopiths. The dietary profiles of some of the extant great apes have been well documented (e.g. Elgart-Berry, 2004; Vogel et al., 2008, 2009, 2014; Yamagiwa and Basabose, 2009; Coiner-Collier et al., 2016). We thus use these profiles to determine whether *G. blacki* had processing capability comparable to those of extant great apes. For instance, if *G. blacki* has higher ACS and absolutely larger BF than *Pongo*, then *G. blacki* teeth were likely capable of withstanding the stresses associated with biting on hard foods, given that some *Pongo* species have been observed to consume hard seeds in the wild (i.e. *Pongo abelii* and *Pongo pygmaeus wurmbii* in the wild; Vogel et al., 2014) and in captivity (e.g. *P. pygmaeus*; Lucas et al., 1994). Australopiths and *G. blacki* have dentognathic traits that have been adaptively linked to processing MCFs, such as robust jaws and thickly-enameled cheek teeth (Teaford and Ungar, 2000; Olejniczak et al., 2008b), yet it is not clear how they differ in their resistance to tooth fracture and BF potential. Therefore, we also compared ACS and BF between *G. blacki* and australopiths.

2. Materials and methods

2.1. Samples

In this study, we focused on mandibular permanent postcanine teeth of *G. blacki*, including four P_3s, four P_4s, four M_1s or M_2s, and four M_3s (Table 1). All samples are isolated teeth and none

show obvious dental pathology. According to the wear stage identification method by Molnar (1971), all teeth studied here are slightly worn, i.e. no wear facets (wear stage = 1) or small wear facets without dentine exposure (wear stage = 2). Only slightly worn teeth (maximum wear stage 2) were deemed suitable for this study as the worn enamel portion needed to be reconstructed in the mesial section prior to estimating ACS and BF, and it would become difficult and less reliable to reconstruct the missing enamel for moderately or heavily worn teeth (wear stage >2). The high degree of morphological similarity between the M_1s and M_2s made it difficult to confidently distinguish between them and thus both positions were provisionally placed into one analytical category ($M_{1/2}$). All teeth were excavated in situ from Bubin basin, Guangxi province, China. Two of these teeth (Z010670 and Z010071) are from Mohui Cave (Wang et al., 2005) and the remaining teeth are from Chuifeng Cave (Wang, 2009). These teeth are now stored in the Anthropology Museum of Guangxi, China.

Comparative data for molar ACS and molar BF were compiled from the literature (Skinner et al., 2015; Chai, 2020; Schwartz et al., 2020) and are provided in SOM Tables S1 and S2. The samples of extant great apes include *Pan paniscus*, *Pan troglodytes*, *Pongo* sp., and *Gorilla* sp. Australopiths include specimens assigned to *Australopithecus anamensis*, *Australopithecus afarensis*, *Australopithecus africanus*, *Paranthropus robustus*, and *Paranthropus boisei*. Species classification and sample sizes (number of permanent molar teeth) are presented in Table 2. Note that the premolar results (ACS and BF) of these comparative taxa were not provided in previous studies, so we only compared the differences for molars. We also did not carry out comparisons for each molar position due to the small sample sizes for many taxa, and instead, M_1–M_3 were pooled for comparisons.

2.2. Data collection

The methods used in this study rely on mesial sections to estimate ACS and BF. To obtain mesial sections, each tooth was scanned using μCT with a 225 kV-μCT scanner at the Institute of Vertebrate Paleontology and Paleoanthropology (IVPP), Chinese Academy of Sciences, with the following parameters: 140 kV, 120 μA, 0.5 angular increment one step, and 360 degrees of rotation. The resultant isometric voxel size (spatial resolution) ranged from 20.39 to 25.90 μm (Table 1). Using IVPP225kVCT_Recon v. 1.0 (IVPP, Beijing), raw projections were converted into image stacks, which were then segmented with the watershed algorithm in Avizo v. 8.0 (www.thermofisher.com). Surface models were generated using the constrained smoothing algorithm with a kernel size of three.

The surface model of a P_3 (Z008545) is shown in Figure 1a to illustrate how the virtual mesial sections were produced. This process was performed in Geomagic Design v. X 64 (www.3dsystems.com). Following the protocols of Tafforeau (2004) and extended by Benazzi et al. (2014), a spline curve was digitized along the cervical line path and then a best fitting plane was produced according to the digitized cervical line. Once this has been accomplished, a mesial section, which is perpendicular to the cervical plane and passing through the two mesial dentine horn tips, can be determined. The resultant mesial section is shown in Figure 1b. For specimens showing slightly worn enamel, the missing enamel was manually reconstructed (Fig. 1c) based on the profiles of unworn teeth (Smith et al., 2012). Skinner et al. (2015) and Lockey et al. (2020) demonstrated that manual enamel reconstruction for slightly worn teeth is generally associated with relatively small error (2.2% and 2.0%, respectively) in 2D enamel thickness measurements. We, therefore, deem the manual reconstruction method to be acceptable in the current study since our main purpose for restoring missing enamel is to measure 2D enamel thickness. Nevertheless, given the subjective nature of enamel reconstruction, different researchers may obtain different

results for a given mesial section. For this reason, the mesial sections prior to reconstruction are provided in SOM Figure S1 to enable other researchers to evaluate the results shown in this work. Following enamel reconstruction, AET (mm) and bi-cervical diameter (BCD, mm) were measured. According to Martin (1985), the expression of AET is shown as:

$$AET = A_{enamel}/L_{edj} \quad (1)$$

where A_{enamel} and L_{edj} are the enamel area (mm^2) and the length (mm) of the EDJ (green dashed line in Fig. 1b), respectively. The calculation of ACS (mm) is shown in Eq. (2) (Schwartz et al., 2020):

$$ACS = (AET \times BCD/2)^{0.5} \quad (2)$$

We measured DHA and cuspal enamel thickness (CET) to estimate BF. Figure 1c illustrates how DHA (φ) is measured. CET (d_c, mm) is the average of three enamel thickness parameters: cuspal inner enamel thickness (d_i, occlusal basin side), cuspal outer enamel thickness (d_o, buccal side for protoconid), and cuspal tip enamel thickness (d_t, the maximum distance between the dentine horn tip and enamel cusp apex; see the illustration in Fig. 1c).

Following Chai (2018), BF (N) can be estimated using the following equation:

$$BF = sA0q^{-1}dc^2 \quad (3)$$

where 's' is a safety factor, defined as the ratio of BF to fracture force (the critical pressure needed to fracture a tooth). Since the safety factor is assumed to be independent of taxon (Chai, 2018), this parameter remains a constant. Chai (2018) calculated the safety factor from a sample of modern human teeth. In the case of modern human molars, in vivo measured average BF was reported as 738 N (Braun et al., 1995; O'Connor et al., 2005) and the estimated average fracture force based on FEA is 1359 N (Chai, 2018). Therefore, the safety factor is approximately equal to 0.55 (s = 738/1359). The parameter A_0 is related to tooth material properties and is expressed as:

$$A_0 = \sigma_F / B \quad (4)$$

$$B \equiv (1 - 2\upsilon_e)/4\pi + 0.72 \log\left[E_e\left(1 - \upsilon_d^2\right)/E_d\left(1 - \upsilon_e^2\right)\right] \quad (5)$$

where σ_F is the peak fracture stress, which occurs slightly below the dentine horn tip, E_e and E_d are the elasticity modulus for enamel and dentine, respectively, and υ_e and υ_d are the Poisson's ratios for enamel and dentine, respectively. The experimental measurements of human tooth properties revealed that the mean values of σ_F, E_e, E_d, υ_e, and υ_d were 118.7 MPa, 90 GPa, 18 GPa, 0.28, and 0.31, respectively (Lees and Rollins, 1972; Xu et al., 1998; Chai, 2014). Substituting these material parameters into Eq. (4) yields A_0 = 224 MPa. To determine the expression of q, Chai (2018) applied FEA to perform a series of numerical simulations, where the force loaded on the tooth cusp remained constant (1 N) while φ varied from 15° to 175° and d_c had four variable choices (0.55, 1.0, 1.5, and 1.9 mm, respectively). By controlling variables, the relationship between q and φ for several choices of d_c can be obtained from the FEA results (Chai, 2018: Fig. 5a). Results showed that q has a polynomial relationship with DHA (Eq. (6)) regardless of the choices of d_c.

$$q = 0.212(1 + a\varphi + b\varphi^2 + c\varphi^3)/(1 + d\varphi + e\varphi^2 + f\varphi^3 + g\varphi^4) \quad (6)$$

$$[a, b, c, d, e, f, g] = 10^{-6}[-23974, 227.95, -0.6569, -26535, 227.95, -1.3058, 0.0023] \quad (7)$$

When the DHA is <150°, q follows a positive trend with increasing dentine angle (Chai, 2018: Fig. 5). Given that the DHA is <150° for most hominid teeth (Chai, 2020), it is assumed that a

positive relationship between φ and q holds in most cases. Since both safety factors and the material-related parameter A_0 are assumed to be independent of taxon, Chai (2018) assumed that BF is mainly controlled by DHA and CET.
For the studied *G. blacki* mesial sections, the buccal dentine horns show conical-like shape while the lingual dentine horns generally do not (e.g. Z008583 in SOM Fig. S1). The method proposed by Chai (2018) is limited to the tooth cusps having conical-like dentine horns, so we measured DHA and CET only on the buccal cusps. Supplementary Online Material Figure S1 displays the buccal cusps in mesial sections and illustrates how DHA and CET were measured for each sample.

2.3. Data analysis
To test for pairwise statistical differences in molar ACS and molar BF between *G. blacki*, extant great apes, and australopiths, we performed nonparametric one-tailed Mann-Whitney (M-W) U-tests, evaluating all possible pairwise differences. We used two-tailed M-W U tests to test for statistical differences in ACS, CET, DHA, q, and BF between premolars (results of P_3 and P_4 were pooled) and molars (results of $M_{1/2}$ and M_3 were pooled) in *G. blacki*. Here, we did not carry out pairwise comparisons for each tooth position because the sample size per tooth position was too small. The Benjamini–Hochberg (B-H) correction was adopted to minimize Type I error for all comparisons (Benjamini and Hochberg, 1995) according to the following two steps. First, all comparisons were ranked by their *p*-values from the smallest to the largest. Second, the original *p*-value for each comparison was corrected by the adjusted *p*-value using the following Eq. (8):

adjusted *p*-value = original *p*-value × *n*/k (8)

adjusted *p*-value = original *p*-value × *n* (9)

adjusted *p*-value = original *p*-value × (*n*-k+1) (10)

where *n* is the total number of comparisons and k is the rank of a given comparison. Compared with the B-H correction, the Bonferroni-type corrections (e.g. standard Bonferroni correction using Eq. (9) and sequential Bonferroni correction using Eq. (10); Holm, 1979; Rice, 1989) are more stringent and may result in rejection of true positive results when there is a large number of comparisons (Benjamini and Hochberg, 1995). As this is likely to be the case in this study, the B-H correction was adopted here. The significance level for all tests was set at $p < 0.05$. All statistical procedures were carried out using Origin v. 9.0 (OriginLab, Northampton).

3. Results

3.1. Absolute crown strength estimates
The results of AET, BCD, and the estimates of ACS for *G. blacki* are provided in Table 3 and Figure 2. Qualitatively, from anterior to posterior along the postcanine tooth row, ACS and AET show subtle increases while BCD basically remains unchanged. Mean P_3 ACS is slightly smaller than that of other tooth positions, while mean P_4 ACS is comparable to that of $M_{1/2}$ and M_3. The average ACS of the premolars (pooled estimate for P_3 and P_4 = 3.811 mm) is approximately equal to that of the molars (pooled estimate for $M_{1/2}$ and M_3 = 3.990 mm). No statistical differences were found between the premolars and molars (M-W U statistic = 25, $Z = -0.683$, $p = 0.505$). Thus, *G. blacki* premolars and molars have comparable resistance to fracture.
There are significant differences in molar ACS among extant great apes, with molar ACS of *Gorilla* being significantly higher than that for *Pongo* and *Pan*, and molar ACS of *Pongo* being significantly higher than that for *Pan* (Fig. 3; Table 4). Within australopiths, all pairwise comparisons of molar ACS show significant differences (Table 4). In ascending order of molar

ACS, these australopiths species are ranked as follows: *A. anamensis* < *A. afarensis* < *A. africanus* < *P. robustus* < *P. boisei* (Fig. 3; Table 4). In comparisons with our sample of extant great apes and australopiths, the molar ACS of *G. blacki* is significantly larger than all taxa except *P. boisei* (Fig. 3; Table 4).

3.2. Bite force estimates

The results of CET, DHA, q, and the estimates of BF potential at each tooth position along the postcanine tooth row for *G. blacki* are provided in Table 5 and Figure 4. Results indicate that BF potential is larger at the premolars than at the molars (Table 5) and is significantly larger at the premolars (pooled estimates) compared with the molars (pooled estimates; M-W U = 55, Z = 2.363, p = 0.015). Moreover, statistical comparisons between the premolars (P_3 and P_4 pooled) and molars ($M_{1/2}$ and M_3 pooled) for *G. blacki* revealed: 1) no significant CET difference (M-W U = 19, $Z = -1.315$; p = 0.185), 2) significant DHA difference (M-W U = 1, $Z = -3.203$, p < 0.001), and 3) significant q difference (M-W U = 1, $Z = -3.203$, $p < 0.001$). Therefore, from anterior to posterior along the postcanine tooth row, CET shows subtle increases (Fig. 4b) and DHA shows significant increases (Fig. 4c). The latter indicates that the dentine horns of premolars are sharper than that of the molars. Corresponding to the variation of DHA, q increases distally (Fig. 4d).

Molar BF comparisons among the nine comparative taxa are provided in Figure 5 and Table 6. Among the extant great apes, *Gorilla gorilla* exhibits the significantly largest molar BF potential while BF potential is significantly larger in *P. pygmaeus* than *P. troglodytes*. All pairwise comparisons among australopiths in molar BF potential are significantly different except between the two *Paranthropus* species, and between *A. anamensis* and *A. afarensis*. The molar BF potential of *Paranthropus* is significantly larger than that of all *Australopithecus* species studied. *Gigantopithecus blacki* shows significantly larger molar BF potential than all extant great apes, *Australopithecus*, and *P. robustus* (Table 6). *Gigantopithecus blacki* and *P. boisei* do not significantly differ in molar BF ($p > 0.05$; Table 6).

4. Discussion and conclusions

4.1. Adaptions of Gigantopithecus blacki *lower postcanine dentition*

Our results show that *G. blacki* has high molar ACS, indicating that its teeth can resist damage caused by intense and/or repeated loading. In addition, the estimated molar BF of *G. blacki* is significantly larger than all species compared except *P. boisei*, suggesting the potential capability of breaching hard objects. Moreover, compared with its molars, *G. blacki* premolars have comparable ACS and larger BF potential. The molarized premolar morphology, with low cusps and relatively flat occlusal basins (Zhang and Harrison, 2017), and the structural properties of crown tissues of *G. blacki* premolars (reflected by ACS and BF, as well as by enamel thickness; Zhang and Zhao, 2013; Pan et al., 2021) may suggest some functional specializations in the premolars. Similar phenomena (but possibly through different evolutionary paths) can be observed in extant primates that primarily feed on tough foods (such as folivores) or hard foods (such as hard-object feeders). For instance, compared to frugivores and insectivores, folivorous primates have statistically larger premolar rows relative to palate area and hard-object feeders generally have larger fourth premolars relative to the first molar (Daegling et al., 2011; Scott et al., 2018).

High ACS and the capacity to generate absolutely large BF along the postcanine dentition, as well as other distinctive dentognathic features, such as an absolutely deep mandibular corpus and relatively thickly-enameled cheek teeth with absolutely large occlusal areas and absolutely long

roots (Woo, 1962; Kupczik and Dean, 2008; Zhang et al., 2014, 2015, 2016) all indicate that *G. blacki* is characterized by a robust masticatory apparatus that has been interpreted as a potential adaptation to processing MCFs.

4.2. Differentiating between tough and hard foods?

Our results allow us to infer that *G. blacki* was capable of processing a wide range of food types including MCFs, but cannot provide direct clues to distinguishing between tough and hard foods or can we say whether *G. blacki* fed opportunistically on MCFs, i.e. as fallback foods when preferred foods were scarce (e.g. Constantino and Wright, 2009; Constantino et al., 2009; Marshall et al., 2009), or whether *G. blacki* fed regularly on MCFs. Differentiation between tough and hard foods can be better appreciated in our study through data on the feeding ecology of extant great apes and through paleodietary inferences of australopiths. First, although *Gorilla* molars show significantly higher ACS and larger estimated BF potential than *Pongo* (Table 4, Table 6; Figure 3, Figure 5), the overall diet of *Gorilla* is generally less resistant to deformation and fracture than that of *Pongo*, as demonstrated by previous studies on food material properties (Elgart-Berry, 2004; Taylor et al., 2008; Vogel et al., 2008, 2014; but see also van Casteren et al., 2019). Second, it is well appreciated that all extant great apes prefer ripe fruits and they switch to more mechanically resistant fallback foods (e.g. tough leaves, bark, and pith) when preferred foods are not available (Vogel et al., 2008, 2009; Yamagiwa and Basabose, 2009; Harrison and Marshall, 2011). This phenomenon suggests that primates may actually avoid those plant tissues to which their masticatory systems are adapted when more nutritious, less mechanically challenging food items are available (Wich et al., 2006; Ungar, 2011, 2019; Grine et al., 2012). Third, our results show that *Australopithecus* and *Paranthropus* have high molar ACS and large estimated molar BF (Figure 3, Figure 5), higher even than *Pongo* (Table 4, Table 6) who are known to feed on hard foods (e.g. *P. pygmaeus wurmbii*; Vogel et al., 2014). The high molar ACS and large estimated BF in *Australopithecus* and *Paranthropus* could thus possibly reflect adaptations for consuming hard foods. However, direct evidence in the form of microwear signatures and tooth chipping left by actual foods eaten generally do not support the routine mastication of hard objects by *Australopithecus* or *P. boisei* (e.g. Ungar et al., 2008, 2010; Ungar, 2011; Ungar and Sponheimer, 2011; Cerling et al., 2011, 2013; Wynn et al., 2013; Constantino and Konow, 2021; Towle et al., 2021). Thus, while our results indicate that *P. boisei* was likely well suited to comminuting hard foods, *P. boisei* teeth have low microwear texture complexity, low to moderate microwear anisotropy values, and low levels of dental chipping, all of which are at odds with the regular consumption of hard objects (Ungar et al., 2008; Cerling et al., 2011; Constantino and Konow, 2021; Towle et al., 2021).

Collectively, high ACS and large BF do not necessarily predict a tougher or harder diet, and they do not necessarily indicate frequent or opportunistic feeding on MCFs. Species with specialized morphologies can have generalized diets or eat more preferred food items when available. This phenomenon, originally documented in a study of African cichlid fishes by Liem (1980), is known as Liem's Paradox (Robinson and Wilson, 1998). It is possible that this phenomenon also characterizes *G. blacki* and australopiths.

4.3. Potential future directions to gain insights into the dietary ecology of Gigantopithecus blacki

Carbon (C) and oxygen (O) isotopic analyses of tooth enamel have suggested that *G. blacki* foraged in densely forested habitat and consumed C_3 plants exclusively (Zhao et al., 2011; Zhao and Zhang, 2013; Nelson, 2014; Qu et al., 2014; Bocherens et al., 2017; Jiang et al., 2021). In this paleoecological context, potential food sources would have been plentiful, leading to speculation

about the foods possibly consumed by *G. blacki*, such as fruits (Woo, 1962; Ciochon et al., 1990; Han and Zhao, 2002; Wang, 2009), tough items (Daegling and Grine, 1994; Zhao and Zhang, 2013), and/or hard objects (Ciochon et al., 1990; Kupczik and Dean, 2008; Qu, 2014; Hu et al., 2022). Previous studies of enamel carbon isotopes and starch grains that bonded to the enamel surface suggest that *G. blacki* may have had a broad dietary range (Qu, 2014; Qu et al., 2014; Nelson, 2014; Bocherens et al., 2017). Our results, specifically the high ACS and large postcanine BF potential, further suggest that *G. blacki* was able to process a broad range of food items including MCFs.

Substantial efforts have been made in previous studies to improve our understanding of *G. blacki* dietary ecology. A recent study presented the Ca isotope data of *G. blacki* and compared it with the data of other 19 taxa, including fauna from the Liucheng *Gigantopithecus* Cave, extant primates, and fossil hominins (Hu et al., 2022). Results revealed that *G. blacki*, *P. boisei*, and the giant panda (*Ailuropoda* sp.) had the highest $\delta^{44/42}$Ca values among the studied taxa. Hu et al. (2022) hypothesized that foraging on mineral licks could be one of the main factors contributing to the high $\delta^{44/42}$Ca values in the enamel of *G. blacki*, *P. boisei*, and the giant panda, which might reflect physiological demands to adapt to feeding on hard foods. While the thick enamel of *P. boisei* was initially interpreted as evidence for durophagy (e.g. Rak, 1983), more recent analyses of dental chipping and microwear patterns of *P. boisei* teeth reveal no evidence of regular hard food consumption (Ungar et al., 2008; Constantino and Konow, 2021; Sponheimer et al., in press). *Ailuropoda* feeds on bamboo, which is a tough food to process (even if some parts of the stem can be hard, they are eaten less often than leaves; Yamashita et al., 2009; King, 2014). Given the paleodietary inferences of *P. boisei* and the tough diet of the giant panda, the high $\delta^{44/42}$Ca values could also reflect feeding on tough foods. Whether *G. blacki* fed on hard foods (regularly or occasionally), tough foods, or both, is still an open question. Further studies of the incidence of dental chipping and microwear analyses in *G. blacki* teeth could provide new insights into this issue.

Declaration of competing interest

The authors declare no conflict of interest.

Acknowledgments

This paper is a tribute to the memory of Lei Pan (IVPP). We thank Song Xing (IVPP) for scanning and technical assistance. This study was supported by the funds from the National Natural Science Foundation of China (Grant No. 42202004 and 42002025), the Major Program of National Social Science Foundation of China (Grant No. 20&ZD246), and the BaGui Scholars Project of the Guangxi Zhuang Autonomous Region, China. We thank co-Editor-in-Chief (Andrea B. Taylor), the Associate Editor, and three reviewers for their comments that greatly improved the manuscript.

References

Begun, D. R., 2010. Miocene hominids and the origins of the African apes and humans. Annu. Rev. Anthropol. 39, 67-84.

Benazzi, S., Panetta, D., Fornai, C., Toussaint, M., Gruppioni, G., Hublin, J. J., 2014. Technical note: Guidelines for the digital computation of 2D and 3D enamel thickness in hominoid teeth. Am. J. Phys. Anthropol. 153, 305-313.

Benjamini, Y., Hochberg Y., 1995. Controlling the false discovery rate: A practical and powerful approach to multiple testing. J. R. Stat. Soc. Ser. B Stat. Methodol. 57, 289-300.

Bocherens, H., Schrenk, F., Chaimanee, Y., Kullmer, O., Morike, D., Pushkina, D., Jaeger, J. J., 2017. Flexibility of diet and habitat in Pleistocene South Asian mammals: Implications for the fate of the giant fossil ape *Gigantopithecus*. Quat. Int. 434, 148-155.

Braun, S., Bantleon, H. P., Hnat, W. P., Freudenthaler, J. W., Marcotte, M. R., Johnson, B. E., 1995. A study of bite force, part 1: Relationship to various physical characteristics. Angle Orthod. 65, 367-372.

Broom, R., Schepers, G. W. H., 1946. The South African fossil ape-men: The Australopithecinae. Trans. Mus. Pret. 2, 1-272.

Cerling, T. E., Mbua, E., Kirera, F. M., Manthi, F. K., Grine, F. E., Leakey, M. G., Sponheimer, M., Uno, K. T., 2011. Diet of *Paranthropus boisei* in the early Pleistocene of East Africa. Proc. Natl. Acad. Sci. USA 108, 9337-9341.

Cerling, T. E., Manthi, F. K., Mbua, E. N., Leakey, L. N., Leakey, M. G., Leakey, R. E., Brown, F. H., Grine, F. E., Hart, J. A., Kaleme, P., Roche, H., Uno, K. T., Wood, B. A., 2013. Stable isotope-based diet reconstructions of Turkana Basin hominins. Proc. Natl. Acad. Sci. USA 110, 10501-10506.

Chai, H., 2014. On the mechanical properties of tooth enamel under spherical indentation. Acta Biomater. 10, 4852-4860.

Chai, H., 2018. Dentin horn angle and enamel thickness interactively control tooth resilience and bite force. Acta Biomater. 75, 279-286.

Chai, H., 2020. Determining primates bite force from histological tooth sections. Am. J. Phys. Anthropol. 171, 683-703.

Ciochon, R., Long, V. T., Larick, R., Gonzalez, L., Grun, R., deVos, J., Yonge, C., Taylor, L., Yoshida, H., Reagan, M., 1996. Dated co-occurrence of *Homo erectus* and *Gigantopithecus* from Tham Khuyen Cave, Vietnam. Proc. Natl. Acad. Sci. USA 93, 3016-3020.

Ciochon, R. L., Piperno, D. R., Thompson, R. G., 1990. Opal phytoliths found on the teeth of extinct ape *Gigantopithecus blacki*: Implications for paleodietary studies. Proc. Natl. Acad. Sci. USA 87, 8120-8124.

Coiner-Collier, S., Scott, R. S., Chalk-Wilayto, J., Cheyne, S. M., Constantino, P., Dominy, N. J., Elgart, A. A., Glowacka, H., Loyola, L. C., Ossi-Lupo, K., Raguet-Schofield, M., Talebi, M. G., Sala, E. A., Sieradzy, P., Taylor, A. B., Vinyard, C. J., Wright, B. W., Yamashita, N., Lucas, P. W., Vogel, E. R., 2016. Primate dietary ecology in the context of food mechanical properties. J. Hum. Evol. 98, 103-118.

Constantino, P. J., Konow, K. A., 2021. Dental chipping supports lack of hard-object feeding in *Paranthropus boisei*. J. Hum. Evol. 156, 103015.

Constantino, P. J., Wright, B. W., 2009. The importance of fallback foods in primate ecology and evolution. Introduction to the symposium issue. Am. J. Phys. Anthropol. 140, 599-602.

Constantino, P. J., Lucas, P. W., Lee, J. J. W., Lawn, B. R., 2009. The influence of fallback foods on great ape tooth enamel. Am. J. Phys. Anthropol. 140, 653-660.

Constantino, P. J., Lee, J. J. W., Chai, H., Zipfel, B., Ziscovici, C., Lawn, B. R., Lucas, P. W., 2010. Tooth chipping can reveal the diet and bite forces of fossil hominins. Biol. Lett. 6, 826-829.

Daegling, D. J., Grine, F. E., 1994. Bamboo feeding, dental microwear, and diet of the Pleistocene ape *Gigantopithecus blacki*. S. Afr. J. Sci. 90, 527-532.

Daegling, D. J., McGraw, W. S., Ungar, P. S., Pampush, J. D., Vick, A. E., Bitty, E. A., 2011. Hard-object feeding in Sooty Mangabeys (*Cercocebus atys*) and interpretation of early hominin feeding ecology. PLoS One 6, e23095.

Demes, B., Creel, N., 1988. Bite force, diet, and cranial morphology of fossil hominids. J. Hum. Evol. 17, 657-670.

Dickson, P., 2003. *Gigantopithecus*: A reappraisal of dietary habits. Univ West. Ont. J. Anthropol. 11, 28-35.
Elgart-Berry, A., 2004. Fracture toughness of mountain gorilla (*Gorilla gorilla beringei*) food plants. Am. J. Primatol. 62, 275-285.
Eng, C. M., Lieberman, D. E., Zink, K. D., Peters, M. A., 2013. Bite force and occlusal stress production in hominin evolution. Am. J. Phys. Anthropol. 151, 544-557.
Gelvin, B. R., 1980. Morphometric affinities of *Gigantopithecus*. Am. J. Phys. Anthropol. 53, 541-568.
Grine, F. E., Sponheimer, M., Ungar, P. S., Lee-Thorp, J., Teaford, M. F., 2012. Dental microwear and stable isotopes inform the paleoecology of extinct hominins. Am. J. Phys. Anthropol. 148, 285-317.
Han, K. X., Zhao, L. X., 2002. Dental caries of *Gigantopithecus blacki* from Hubei province of China. Acta Anthropol. Sin. 21, 191-197.
Harrison, M. E., Marshall, A. J., 2011. Strategies for the use of fallback foods in apes. Int. J. Primatol. 32, 531-565.
Holm, S., 1979. A simple sequentially rejective multiple test procedure. Scand. J. Stat. 6, 65-70.
Hu, Y., Jiang, Q., Liu, F., Guo, L., Zhang, Z., Zhao, L., 2022. Calcium isotope ecology of early *Gigantopithecus blacki* (~2 Ma) in South China. Earth Planet. Sci. Lett. 584, 117522.
Jiang, Q. Y., Zhao, L. X., Guo, L., Hu, Y. W., 2021. First direct evidence of conservative foraging ecology of early *Gigantopithecus blacki* (similar to 2 Ma) in Guangxi, southern China. Am. J. Phys. Anthropol. 176, 93-108.
Jin, C. Z., Qin, D. G., Pan, W. S., Tang, Z. L., Liu, J. Y., Wang, Y., Deng, C. L., Zhang, Y. Q., Dong, W., Tong, H. W., 2009. A newly discovered *Gigantopithecus* fauna from Sanhe Cave, Chongzuo, Guangxi, South China. Chin. Sci. Bull. 54, 788-797.
Jin, C. Z., Wang, Y., Deng, C. L., Harrison, T., Qin, D. G., Pan, W. S., Zhang, Y. Q., Zhu, M., Yan, Y. L., 2014. Chronological sequence of the early Pleistocene *Gigantopithecus* faunas from cave sites in the Chongzuo, Zuojiang River area, South China. Quat. Int. 354, 4-14.
King, R. A., 2014. Using *Ailuropoda melanoleuca* as a model species for studying the ecomorphology of *Paranthropus*. MA. Sc. Dissertation, Marshall University.
Kono, R. T., Zhang, Y. Q., Jin, C. Z., Takai, M., Suwa, G., 2014. A 3-dimensional assessment of molar enamel thickness and distribution pattern in *Gigantopithecus blacki*. Quat. Int. 354, 46-51.
Kupczik, K., Dean, M. C., 2008. Comparative observations on the tooth root morphology of *Gigantopithecus blacki*. J. Hum. Evol. 54, 196-204.
Lawn, B. R., Lee, J. J. W., 2009. Analysis of fracture and deformation modes in teeth subjected to occlusal loading. Acta Biomater. 5, 2213-2221.
Lees, S., Rollins, F. R., 1972. Anisotropy in hard dental tissues. J. Biomech. 15, 557-566.
Liem, K. F., 1980. Adaptive significance of intraspecific and interspecific differences in the feeding repertoires of cichlid fishes. Am. Zool. 20, 295-314.
Lockey, A. L., Alemseged, Z., Hublin, J. J., Skinner, M. M., 2020. Maxillary molar enamel thickness of Plio-Pleistocene hominins. J. Hum. Evol. 142, 102731.
Lucas, P. W., Peters, C. R., Arrandale, S. R., 1994. Seed-breaking forces exerted by orang-utans with their teeth in captivity and a new technique for estimating forces produced in the wild. Am. J. Phys. Anthropol. 94, 365-378.
Marshall, A. J., Boyko, C. M., Feilen, K. L., Boyko, R. H., Leighton, M., 2009. Defining fallback foods and assessing their importance in primate ecology and evolution. Am. J. Phys. Anthropol. 140, 603-614.

Martin, L. B., 1985. Significance of enamel thickness in hominoid evolution. Nature 314, 260-263.
Miller, S. F., White, J. L., Ciochon, R. L., 2008. Assessing mandibular shape variation within *Gigantopithecus* using a geometric morphometric approach. Am. J. Phys. Anthropol. 137, 201-212.
Molnar, S., 1971. Human tooth wear, tooth function and cultural variability. Am. J. Phys. Anthropol. 34, 175-189.
Nelson, S. V., 2014. The paleoecology of Early Pleistocene *Gigantopithecus blacki* inferred from isotopic analyses. Am. J. Phys. Anthropol. 155, 571-578.
Noerwidi, S., Siswanto, Widianto, H., 2016. Giant primate of Java: A new *Gigantopithecus* specimen from Semedo. Berkala Arkeologi 36, 141-160.
O'Connor, C. F., Franciscus, R. G., Holton, N. E., 2005. Bite force production capability and efficiency in Neandertals and modern humans. Am. J. Phys. Anthropol. 127, 129-151.
Olejniczak, A. J., Smith, T. M., Wang, W., Potts, R., Ciochon, R., Kullmer, O., Schrenk, F., Hublin, J. J., 2008a. Molar enamel thickness and dentine horn height in *Gigantopithecus blacki*. Am. J. Phys. Anthropol. 135, 85-91.
Olejniczak, A. J., Smith, T. M., Skinner, M. M., Grine, F. E., Feeney, R. N. M., Thackeray, J. F., Hublin, J. J., 2008b. Three-dimensional molar enamel distribution and thickness in *Australopithecus* and *Paranthropus*. Biol. Lett. 4, 406-410.
Pan, L., Ji, X. P., Liao, W., Wang, W., Liu, J. H., Xing, S., 2021. Premolar enamel thickness and distribution of a Miocene hominid *Lufengpithecus hudienensis* compared with Pleistocene and extant hominids. J. Hum. Evol. 157, 103030.
Pei, W. C., Woo, J. K., 1956. New materials of *Gigantopithecus* teeth from South China. Acta Anthropol. Sin. 4, 477-490.
Pilbeam, D., 1970. *Gigantopithecus* and the origins of Hominidae. Nature 225, 516-519.
Qu, Y. T., 2014. Dietary behaviors of *Gigantopithecus blacki* and their potential impact on the evolution of *G. blacki*. Ph. D. Dissertation, Institute of Vertebrate Paleontology and Paleoanthropology, Beijing.
Qu, Y. T., Jin, C. Z., Zhang, Y. Q., Hu, Y. W., Shang, X., Wang, C. S., 2014. Preservation assessments and carbon and oxygen isotopes analysis of tooth enamel of *Gigantopithecus blacki* and contemporary animals from Sanhe Cave, Chongzuo, South China during the Early Pleistocene. Quat. Int. 354, 52-58.
Rice, W. R., 1989. Analyzing tables of statistical tests. Evolution 43, 223-225.
Robinson, B. W., Wilson, D. S., 1998. Optimal foraging, specialization, and a solution to Liem's paradox. Am. Nat. 151, 223-235.
Schwartz, G. T., McGrosky, A., Strait, D. S., 2020. Fracture mechanics, enamel thickness and the evolution of molar form in hominins. Biol. Lett. 16, 20190671.
Scott, J. E., Campbell, R. M., Baj, L. M., Burns, M. C., Price, M. S., Sykes, J. D., Vinyard, C. J., 2018. Dietary signals in the premolar dentition of primates. J. Hum. Evol. 121, 221-234.
Shao, Q. F., Wang, W., Deng, C. L., Voinchet, P., Lin, M., Zazzo, A., Douville, E., Dolo, J. M., Falgueres, C., Bahain, J. J., 2014. ESR, U-series and paleomagnetic dating of *Gigantopithecus* fauna from Chuifeng Cave, Guangxi, southern China. Quat. Res. 82, 270-280.
Shao, Q. F., Bahain, J. J., Wang, W., Zhu, M., Voinchet, P., Lin, M., Douville, E., 2015. Coupled ESR and U-series dating of early Pleistocene *Gigantopithecus* faunas at Mohui and Sanhe Caves, Guangxi, southern China. Quat. Geochronol. 30, 524-528.
Shao, Q. F., Wang, Y., Voinchet, P., Zhu, M., Lin, M., Rink, W. J., Jin, C. Z., Bahain, J. J., 2017. U-series and ESR/U-series dating of the *Stegodon-Ailuropoda* fauna at Black Cave, Guangxi,

southern China with implications for the timing of the extinction of *Gigantopithecus blacki*. Quat. Int. 434, 65-74.
Skinner, M. M., Alemseged, Z., Gaunitz, C., Hublin, J. J., 2015. Enamel thickness trends in Plio-Pleistocene hominin mandibular molars. J. Hum. Evol. 85, 35-45.
Smith, T. M., Kupczik, K., Machanda, Z., Skinner, M. M., Zermeno, J. P., 2012. Enamel thickness in Bornean and Sumatran orangutan dentitions. Am. J. Phys. Anthropol. 147, 417-426.
Sponheimer, M., Daegling, D. J., Ungar, P. S., Bobe, R., Paine, Oliver C. C., 2022. Problems with *Paranthropus*. Quat. Int. in press.
Sun, L., Wang, Y., Liu, C. C., Zuo, T. W., Ge, J. Y., Zhu, M., Jin, C. Z., Deng, C. L., Zhu, R. X., 2014. Magnetochronological sequence of the Early Pleistocene *Gigantopithecus* faunas in Chongzuo, Guangxi, southern China. Quat. Int. 354, 15-23.
Tafforeau, P., 2004. Phylogenetic and functional aspects of tooth enamel microstructure and three-dimensional structure of modern and fossil primate molars. Ph. D. Dissertation, Universite de Montpellier II.
Taylor, A. B., 2006. Feeding behavior, diet, and the functional consequences of jaw form in orangutans, with implications for the evolution of *Pongo*. J. Hum. Evol. 50, 377-393.
Taylor, A. B., Vogel, E. R., Dominy, N. J., 2008. Food material properties and mandibular load resistance abilities in large-bodied hominoids. J. Hum. Evol. 55, 604-616.
Teaford, M. F., Ungar, P. S., 2000. Diet and the evolution of the earliest human ancestors. Proc. Natl. Acad. Sci. USA 97, 13506-13511.
Towle, I., Irish, J. D., Loch, C., 2021. *Paranthropus robustus* tooth chipping patterns do not support regular hard food mastication. J. Hum. Evol. 158, 103044.
Ungar, P. S., 2011. Dental evidence for the diets of Plio-Pleistocene hominins. Am. J. Phys. Anthropol. 146, 47-62.
Ungar, P. S., 2019. Inference of diets of early hominins from orimate molar form and microwear. J. Dent. Res. 98, 398-405.
Ungar, P. S., Sponheimer, M., 2011. The diets of early hominins. Science 334, 190-193.
Ungar, P. S., Grine, F. E., Teaford, M. F., 2008. Dental microwear and diet of the Plio-Pleistocene hominin *Paranthropus boisei*. PLoS One 3, e2044.
Ungar, P. S., Scott, R. S., Grine, F. E., Teaford, M. F., 2010. Molar microwear textures and the diets of *Australopithecus anamensis* and *Australopithecus afarensis*. Philos. Trans. R. Soc. B Biol. Sci. 365, 3345-3354.
van Casteren, A., Wright, E., Kupczik, K., Robbins, M. M., 2019. Unexpected hard-object feeding in Western lowland gorillas. Am. J. Phys. Anthropol. 170, 433-438.
Vogel, E. R., van Woerden, J. T., Lucas, P. W., Atmoko, S. S. U., van Schaik, C. P., Dominy, N. J., 2008. Functional ecology and evolution of hominoid molar enamel thickness: *Pan troglodytes schweinfurthii* and *Pongo pygmaeus wurmbii*. J. Hum. Evol. 55, 60-74.
Vogel, E. R., Haag, L., Mitra-Setia, T., van Schaik, C. P., Dominy, N. J., 2009. Foraging and ranging behavior during a fallback episode: *Hylobates albibarbis* and *Pongo pygmaeus wurmbii* compared. Am. J. Phys. Anthropol. 140, 716-726.
Vogel, E. R., Zulfa, A., Hardus, M., Wich, S. A., Dominy, N. J., Taylor, A. B., 2014. Food mechanical properties, feeding ecology, and the mandibular morphology of wild orangutans. 75, 110-124.
Von Koenigswald, G. H. R., 1935. Eine fossile Säugetierfauna mit Simiaaus Südchina. Proc. Kon. Ned. Akad. Wetensch. Ser. B 38, 872-879.
Wang, W., 2009. New discoveries of *Gigantopithecus blacki* teeth from Chuifeng Cave in the Bubing Basin, Guangxi, south China. J. Hum. Evol. 57, 229-240.

Wang, W., Potts, R., Hou, Y. M., Chen, Y. F., Wu, H. Y., Yuan, B. Y., Huang, W. W., 2005. Early Pleistocene hominid teeth recovered in Mohui cave in Bubing Basin, Guangxi, South China. Chin. Sci. Bull. 50, 2777-2782.

Wang, Y., Jin, C. Z., Pan, W. S., Qin, D. G., Yan, Y. L., Zhang, Y. Q., Liu, J. Y., Dong, W., Deng, C. L., 2017. The Early Pleistocene *Gigantopithecus-Sinomastodon* fauna from Juyuan karst cave in Boyue Mountain, Guangxi, South China. Quat. Int. 434, 4-16.

Weidenreich, F., 1945. Giant early man from Java and South China. Anthropol. Pap. Am. Mus. Nat. Hist. 40, 1-134.

Welker, F., Ramos-Madrigal, J., Kuhlwilm, M., Liao, W., Gutenbrunner, P., de Manuel, M., Samodova, D., Mackie, M., Allentoft, M. E., Bacon, A. M., Collins, M. J., Cox, J., Lalueza-Fox, C., Olsen, J. V., Demeter, F., Wang, W., Marques-Bonet, T., Cappellini, E., 2019. Enamel proteome shows that *Gigantopithecus* was an early diverging pongine. Nature 576, 262-265.

Woo, J. K., 1962. The mandibles and dentition of *Gigantopithecus*. Palaeontol. Sin. New Ser. D 11, 1-94.

Wich, S. A., Utami-Atmoko, S. S., Setia, T. M., Djoyosudharmo, S., Geurts, M. L., 2006. Dietary and energetic responses of *Pongo abelii* to fruit availability fluctuations. Int. J. Primatol. 27, 1535-1550.

Wroe, S., Ferrara, T. L., McHenry, C. R., Curnoe, D., Chamoli, U., 2010. The craniomandibular mechanics of being human. Proc. R. Soc. B Biol. Sci. 277, 3579-3586.

Wynn, J. G., Sponheimer, M., Kimbel, W. H., Alemseged, Z., Reed, K., Bedaso, Z. K., Wilson, J. N., 2013. Diet of *Australopithecus afarensis* from the Pliocene Hadar Formation, Ethiopia. Proc. Natl. Acad. Sci. USA 110, 10495-10500.

Xu, H. H. K., Smith, D. T., Jahanmir, S., Romberg, E., Kelly, J. R., Thompson, V. P., Rekow, E. D., 1998. Indentation damage and mechanical properties of human enamel and dentin. J. Dent. Res. 77, 472-480.

Yamagiwa, J., Basabose, A. K., 2009. Fallback foods and dietary partitioning among *Pan* and *Gorilla*. Am. J. Phys. Anthropol. 140, 739-750.

Zanolli, C., Kullmer, O., Kelley, J., Bacon, A. M., Demeter, F., Dumoncel, J., Fiorenza, L., Grine, F. E., Hublin, J. J., Nguyen, A. T., Nguyen, T. M. H., Pan, L., Schillinger, B., Schrenk, F., Skinner, M. M., Ji, X. P., Macchiarelli, R., 2019. Evidence for increased hominid diversity in the Early to Middle Pleistocene of Indonesia. Nat. Ecol. Evol. 3, 755-764.

Zhang, L. Z., Zhao, L. X., 2013. Enamel thickness of *Gigantopithecus blacki* and its significance for dietary adaptation and phylogeny. Acta Anthropol. Sin. 32, 365-376.

Zhang, Y. Q., Harrison, T., 2017. *Gigantopithecus blacki*: A giant ape from the Pleistocene of Asia revisited. Am. J. Phys. Anthropol. 162, 153-177.

Zhang, Y. Q., Jin, C. Z., Cai, Y. J., Kono, R. K., Wang, W., Wang, Y., Zhu, M., Yan, Y. L., 2014. New 400-320 ka *Gigantopithecus blacki* remains from Hejiang Cave, Chongzuo City, Guangxi, South China. Quat. Int. 354, 35-45.

Zhang, Y. Q., Kono, R. T., Wang, W., Harrison, T., Takai, M., Ciochon, R. L., Jin, C. Z., 2015. Evolutionary trend in dental size in *Gigantopithecus blacki* revisited. J. Hum. Evol. 83, 91-100.

Zhang, Y. Q., Jin, C. Z., Kono, R. T., Harrison, T., Wang, W., 2016. A fourth mandible and associated dental remains of *Gigantopithecus blacki* from the Early Pleistocene Yanliang Cave, Fusui, Guangxi, South China. Hist. Biol. 28, 95-104.

Zhang, Y. Y., 1982. Variability and evolutionary trends in tooth size of *Gigantopithecus blacki*. Am. J. Phys. Anthropol. 59, 21-32.

Zhao, L. X., Zhang, L. Z., 2013. New fossil evidence and diet analysis of *Gigantopithecus blacki* and its distribution and extinction in South China. Quat. Int. 286, 69-74.

Zhao, L. X., Zhang, L. Z., Zhang, F. S., Wu, X. Z., 2011. Enamel carbon isotope evidence of diet and habitat of *Gigantopithecus blacki* and associated mammalian megafauna in the Early Pleistocene of South China. Chin. Sci. Bull. 56, 3590-3595.

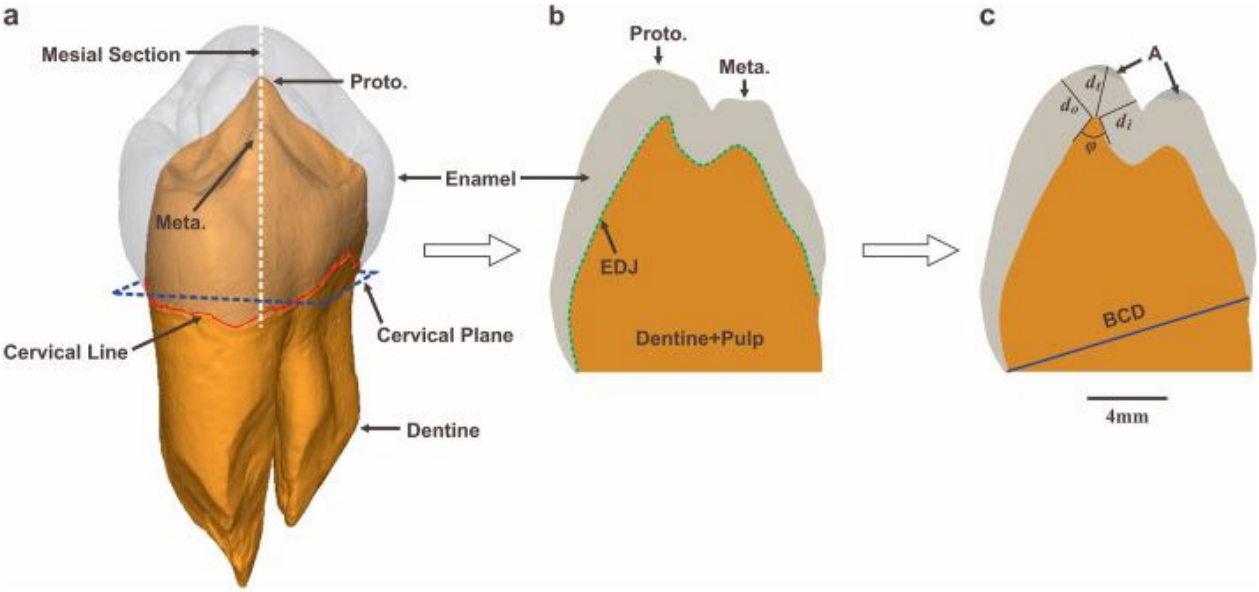

Figure 1. a) Virtual three-dimensional reconstruction of a *Gigantopithecus blacki* third premolar (Z008545). The enamel is rendered in semitransparency, showing the underlying enamel-dentine junction surface. The white dashed line indicates mesial section position. b) Virtual mesial section is produced following the general protocol (Benazzi et al., 2014; Tafforeau, 2004). c) Illustration of restoring missing enamel (dark zone pointed by arrows from A), measuring bi-cervical diameter (BCD), dentine horn angle (φ), and cuspal enamel thickness parameters (d_i, d_o, and d_t). Abbreviations: Proto. = protoconid; Meta. = metaconid.

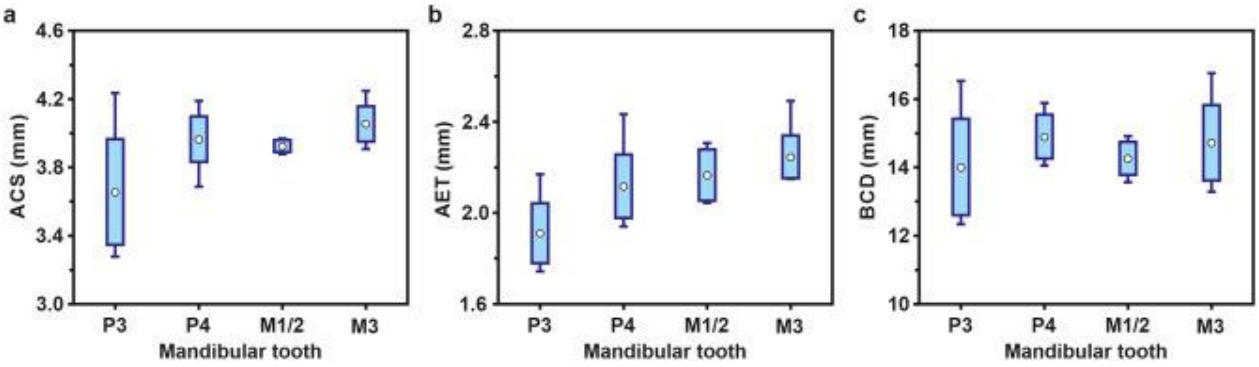

Figure 2. Box plots of a) absolute crown strength (ACS), b) average enamel thickness (AET), and c) bi-cervical diameter (BCD) for *Gigantopithecus* mandibular premolars and molars. The premolars (especially P_4) have ACS that are comparable to the molars.

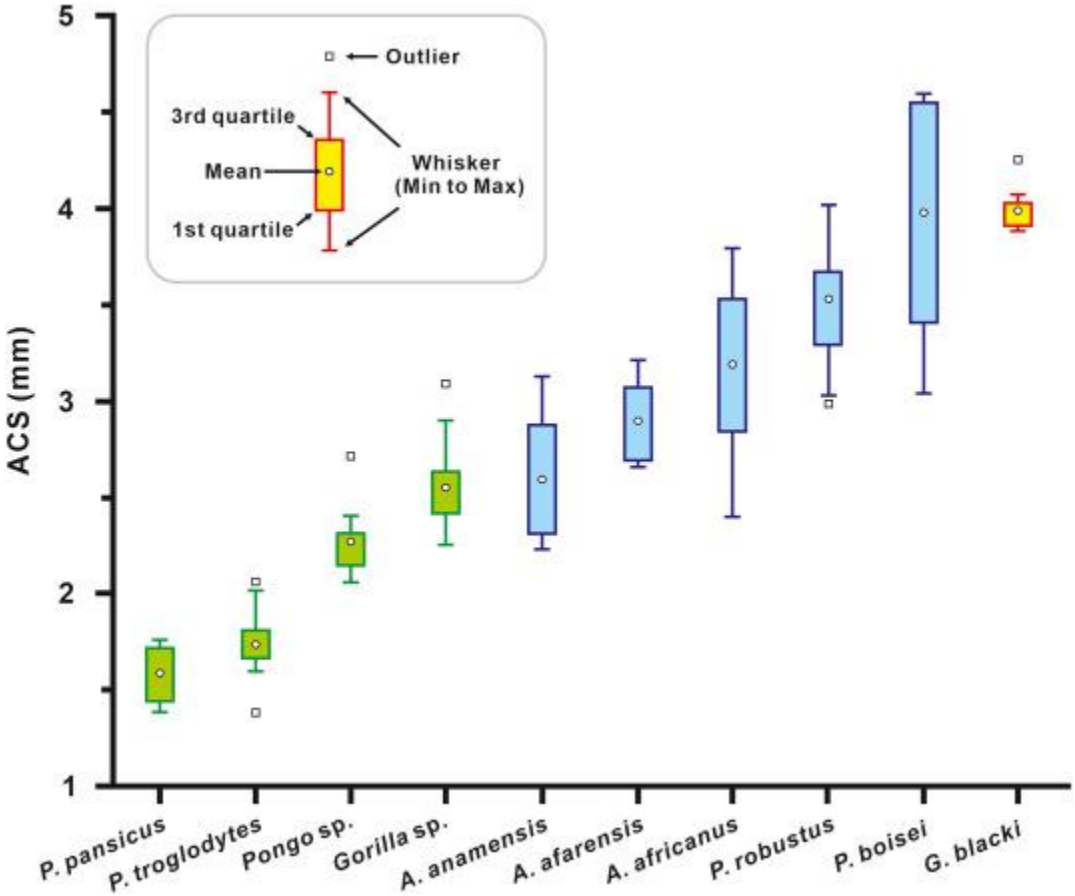

Figure 3. Box plots of molar absolute crown strength (ACS) for *Gigantopithecus blacki* (yellow box), australopiths (blue boxes), and extant great apes (green boxes). Except for *G. blacki*, the ACS results for the other taxa were extracted from Schwartz et al. (2020). *Gigantopithecus blacki* has significantly higher ACS than most taxa (see Table 4).

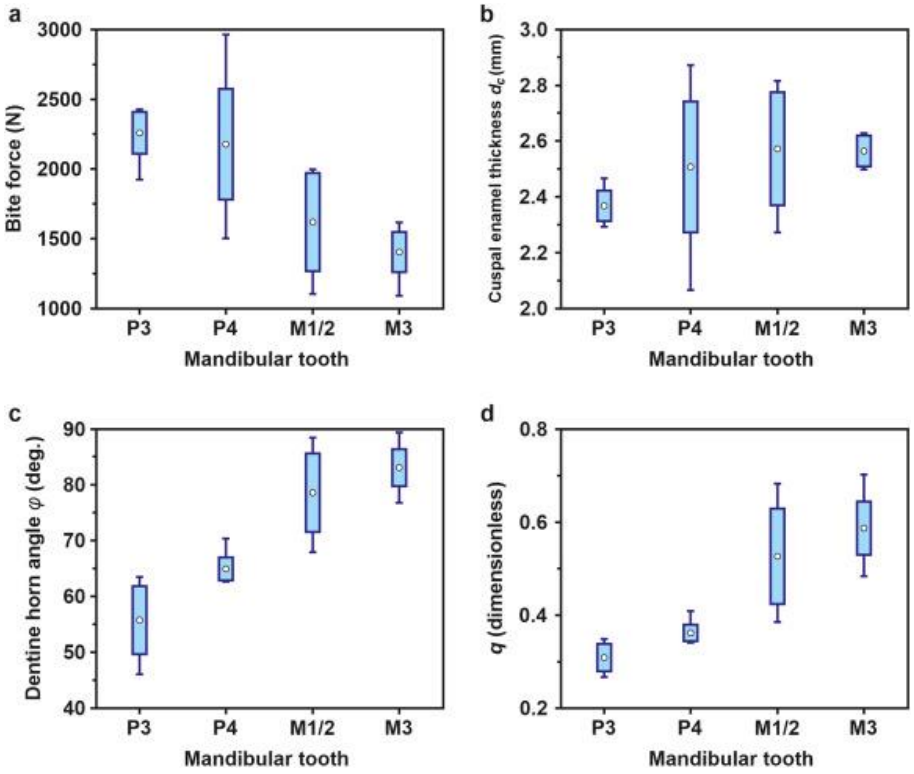

Figure 4. Box plots of a) bite force, b) cuspal enamel thickness, c) dentine horn angle, and d) configuration parameter q for *Gigantopithecus* mandibular premolars and molars. The premolars have larger BF than the molars do.

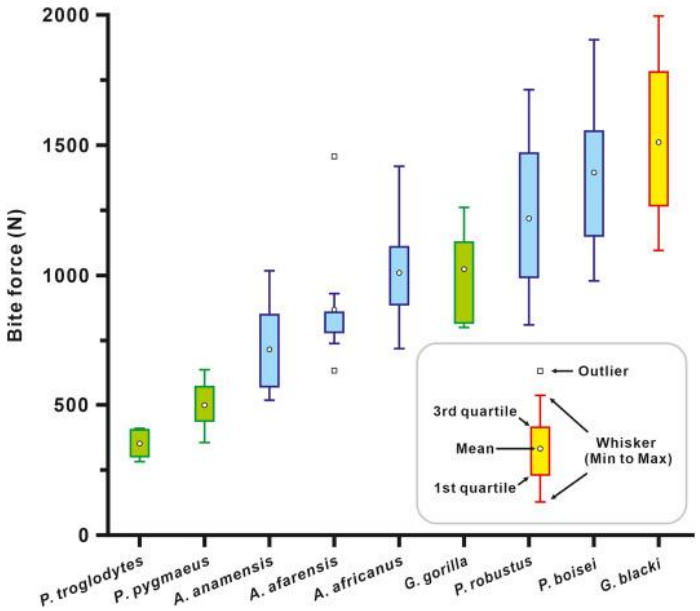

Figure 5. Box plots of molar bite force (BF) for *Gigantopithecus blacki* (yellow box), australopiths (blue boxes), and extant great apes (green boxes). Except for *G. blacki*, the BF data for the other taxa were extracted from Chai (2020). *Gigantopithecus blacki* has significantly larger BF than most taxa (see Table 6).

Table 1
Sample of *Gigantopithecus blacki* teeth studied in this work.

Specimen	Tooth	Wear[a]	Voxel size (μm)	Provenance[b]	Age (Ma)	References
Z008545	LP_3	2	25.90	CF	1.97 ± 0.19–1.38 ± 0.17 (Early Pleistocene)	Wang (2009); Shao et al. (2014)
Z008547	LP_3	2	23.50	CF		Wang (2009); Shao et al. (2014)
Z008549	LP_3	2	25.90	CF		Wang (2009); Shao et al. (2014)
Z008551	LP_3	2	25.90	CF		Wang (2009); Shao et al. (2014)
Z008553	LP_4	2	25.90	CF		Wang (2009); Shao et al. (2014)
Z008562	RP_4	2	25.90	CF		Wang (2009); Shao et al. (2014)
Z008558	LP_4	1	25.90	CF		Wang (2009); Shao et al. (2014)
Z008563	RP_4	2	25.90	CF		Wang (2009); Shao et al. (2014)
Z008564	$LM_{1/2}$	2	25.09	CF		Wang (2009); Shao et al. (2014)
Z008566	$LM_{1/2}$	2	25.09	CF		Wang (2009); Shao et al. (2014)
Z008572	$LM_{1/2}$	2	25.90	CF		Wang (2009); Shao et al. (2014)
Z010670	$LM_{1/2}$	2	20.39	MH	1.69 ± 0.22–1.29 ± 0.11 (Early Pleistocene)	Wang et al. (2005); Shao et al. (2015)
Z010071	LM_3	2	20.39	MH		Wang et al. (2005); Shao et al. (2015)
Z010654	LM_3	2	23.50	CF	1.97 ± 0.19–1.38 ± 0.17 (Early Pleistocene)	Wang (2009); Shao et al. (2014)
Z008581	LM_3	2	23.50	CF		Wang (2009); Shao et al. (2014)
Z008583	RM_3	2	23.50	CF		Wang (2009); Shao et al. (2014)

Abbreviations: L = left; R = right; CF = Chuifeng Cave; MF = Mohui Cave.
[a] Occlusal wear stage was assessed in line with Molnar (1971).
[b] Both Chuifeng and Mohui are located in Tiandong, Guangxi province, China.

Table 2
Extant ape and australopith comparative data for molar absolute crown strength (ACS) and molar bite force (BF) included in this study[a].

Taxon	Sample size	Estimated ACS/BF (Mean ± standard deviation)	Reference
ACS (mm) comparisons			
Pan paniscus	8	1.59 ± 0.15	Schwartz et al. (2020)
Pan troglodytes	16	1.74 ± 0.16	
Pongo sp.	9	2.28 ± 0.20	
Gorilla sp.	13	2.56 ± 0.23	
Australopithecus anamensis	13	2.60 ± 0.29	
Australopithecus afarensis	8	2.90 ± 0.21	
Australopithecus africanus	31	3.20 ± 0.37	
Paranthropus robustus	24	3.53 ± 0.27	
Paranthropus boisei	7	3.98 ± 0.58	
BF (N) comparisons			
Pan troglodytes[b]	4	354 ± 53	Chai (2020)
Pongo pygmaeus	9	500 ± 83	
Gorilla gorilla	5	1023 ± 184	
Australopithecus anamensis	8	715 ± 182	
Australopithecus afarensis	9	865 ± 222	
Australopithecus africanus	15	1017 ± 197	
Paranthropus robustus	17	1220 ± 284	
Paranthropus boisei	9	1396 ± 307	

[a] Measurement details of ACS and BF are provided in Schwartz et al. (2020) and Chai (2020), respectively.
[b] Updated results (Chai, pers. commun., 2022).

Table 3

Results of enamel area, enamel-dentine junction (EDJ) length, average enamel thickness (AET), and bi-cervical diameter (BCD) used to compute the absolute crown strength (ACS) index for *Gigantopithecus blacki* lower premolars and molars.

Specimen	Tooth	Enamel area (mm^2)	EDJ length (mm)	AET (mm)	BCD (mm)	ACS (mm)	Mean ACS (mm)
Z008545	P_3	52.156	28.702	1.817	12.847	3.416	3.657
Z008547		51.846	29.739	1.743	12.338	3.279	
Z008549		76.770	35.385	2.170	16.524	4.234	
Z008551		60.604	31.639	1.915	14.288	3.699	
Z008553	P_4	77.133	38.178	2.020	15.878	4.005	3.964
Z008562		60.164	31.062	1.937	14.050	3.689	
Z008558		83.262	34.230	2.432	14.441	4.191	
Z008563		63.444	30.542	2.077	15.200	3.973	
Z008564	$M_{1/2}$	67.566	29.284	2.307	13.556	3.954	3.925
Z008566		62.280	27.699	2.248	13.987	3.965	
Z008572		53.073	25.718	2.064	14.567	3.877	
Z010670		60.983	29.843	2.043	14.908	3.903	
Z010071	M_3	56.448	26.259	2.150	14.878	3.999	4.055
Z010654		61.537	24.707	2.491	13.285	4.067	
Z008581		64.322	29.855	2.154	16.746	4.247	
Z008583		58.985	26.960	2.188	13.946	3.906	

Table 4
Results of pairwise comparisons for differences in molar absolute crown strength (ACS) among species. *P*-values are presented below the diagonal and directional differences are presented above the diagonal[a, b].

Taxon	*Pan pansicus*	*Pan troglodytes*	*Pongo*	*Gorilla*	*A. anamensis*	*A. afarensis*	*A. africanus*	*P. robustus*	*P. boisei*	*G. blacki*
Pan pansicus		Ppa < Ptr	Ppa < Pon	Ppa < Gor	Ppa < Aan	Ppa < Aafa	Ppa < Aafr	Ppa < Pro	Ppa < Pbo	Ppa < Gbl
Pan troglodytes	**0.037**		Ptr < Pon	Ptr < Gor	Ptr < Aan	Ptr < Aafa	Ptr < Aafr	Ptr < Pro	Ptr < Pbo	Ptr < Gbl
Pongo	**<0.001**	**<0.001**		Pon < Gor	Pon < Aan	Pon < Aafa	Pon < Aafr	Pon < Pro	Pon < Pbo	Pon < Gbl
Gorilla	**<0.001**	**<0.001**	**0.002**		NSD	Gor < Aafa	Gor < Aafr	Gor < Pro	Gor < Pbo	Gor < Gbl
A. anamensis	**<0.001**	**<0.001**	**0.004**	0.381		Aan < Aafa	Aan < Aafr	Aan < Pro	Aan < Pbo	Aan < Gbl
A. afarensis	**<0.001**	**<0.001**	**<0.001**	**0.001**	**0.014**		Aafa < Aafr	Aafa < Pro	Aafa < Pbo	Aafa < Gbl
A. africanus	**<0.001**	**<0.001**	**<0.001**	**<0.001**	**<0.001**	**0.013**		Aafr < Pro	Aafr < Pbo	Aafr < Gbl
P. robustus	**<0.001**	**<0.001**	**<0.001**	**<0.001**	**<0.001**	**<0.001**	**0.001**		Pro < Pbo	Pro < Gbl
P. boisei	**<0.001**	**<0.001**	**<0.001**	**<0.001**	**<0.001**	**<0.001**	**0.002**	**0.029**		NSD
G. blacki	**<0.001**	**<0.001**	**<0.001**	**<0.001**	**<0.001**	**<0.001**	**<0.001**	**<0.001**	0.732	

[a] Bold *p*-values indicate significant differences in molar ACS following the Benjamini-Hochberg adjustment. NSD = nonsignificant difference prior to the Benjamini-Hochberg adjustment.
[b] Ppa = *Pan pansicus*; Ptr = *Pan troglodytes*; Pon = *Pongo*; Gor = *Gorilla*; Aan = *Australopithecus anamensis*; Aafa = *Australopithecus afarensis*; Aafr = *Australopithecus africanus*; Pro = *Paranthropus robustus*; Pbo = *Paranthropus boisei*; Gbl = *Gigantopithecus blacki*.

Table 5
Results of cuspal enamel thickness (d_c) and dentine horn angle (φ) used to estimate bite force (BF) for *Gigantopithecus blacki* lower premolars and molars[a].

Specimen	Tooth	d_c (mm)	φ (degree)	q	BF (N)	Mean BF (N)
Z008545	P_3	2.34	63.48	0.35	1925.52	2258.31
Z008547		2.29	46.06	0.27	2427.25	
Z008549		2.47	60.19	0.33	2292.48	
Z008551		2.38	53.32	0.29	2388.01	
Z008553	P_4	2.07	63.69	0.35	1502.20	2177.57
Z008562		2.61	70.39	0.41	2059.13	
Z008558		2.87	62.68	0.34	2960.74	
Z008563		2.48	63.00	0.34	2188.20	
Z008564	$M_{1/2}$	2.73	75.05	0.46	1996.60	1619.53
Z008566		2.82	88.47	0.68	1430.04	
Z008572		2.27	82.79	0.58	1104.49	
Z010670		2.47	67.98	0.38	1946.98	
Z010071	M_3	2.63	82.76	0.58	1478.15	1405.20
Z010654		2.61	83.38	0.59	1431.23	
Z008581		2.52	76.76	0.48	1617.65	
Z008583		2.50	89.41	0.70	1093.76	

[a] q is a parameter that has a polynomial relationship with dentine horn angle.

Table 6

Results of pairwise comparisons for differences in molar bite force (BF) among species. *P*-values are presented below the diagonal and directional differences are presented above the diagonal[a, b].

Taxon	*Pan troglodytes*	*Pongo pygmaeus*	*A. anamensis*	*A. afarensis*	*A. africanus*	*Gorilla gorilla*	*P. robustus*	*P. boisei*	*G. blacki*
Pan troglodytes		Ptr < Ppy	Ptr < Aan	Ptr < Aafa	Ptr < Aafr	Ptr < Ggo	Ptr < Pro	Ptr < Pbo	Ptr < Gbl
Pongo pygmaeus	**0.009**		Ppy < Aan	Ppy < Aafa	Ppy < Aafr	Ppy < Ggo	Ppy < Pro	Ppy < Pbo	Ppy < Gbl
A. anamensis	**0.003**	**0.003**		NSD	Aan < Aafr	Aan < Ggo	Aan < Pro	Aan < Pbo	Aan < Gbl
A. afarensis	**0.003**	**<0.001**	0.057		Aafa < Aafr	NSD	Aafa < Pro	Aafa < Pbo	Aafa < Gbl
A. africanus	**<0.001**	**<0.001**	**0.002**	**0.040**		NSD	Aafr < Pro	Aafr < Pbo	Aafr < Gbl
Gorilla gorilla	**0.012**	**0.001**	**0.013**	0.073	0.359		NSD	Ggo < Pbo	Ggo < Gbl
P. robustus	**<0.001**	**<0.001**	**<0.001**	**0.002**	**0.028**	0.109		NSD	Ggo < Gbl
P. boisei	**0.003**	**<0.001**	**<0.001**	**0.002**	**0.002**	**0.038**	0.132		NSD
G. blacki	**0.003**	**<0.001**	**<0.001**	**0.001**	**<0.001**	**0.030**	**0.050**	0.212	

[a] Bold *p*-values indicate significant differences in molar BF following the Benjamini-Hochberg adjustment. NSD = nonsignificant difference prior to the Benjamini-Hochberg adjustment.

[b] Ptr = *Pan troglodytes*; Pon = *Pongo*; Gor = *Gorilla*; Aan = *Australopithecus anamensis*; Aafa = *Australopithecus afarensis*; Aafr = *Australopithecus africanus*; Pro = *Paranthropus robustus*; Pbo = *Paranthropus boisei*; Gbl = *Gigantopithecus blacki*.